PAPER

Biofabrication of human articular cartilage: a path towards the development of a clinical treatment

Biofabrication

PAPER

Biofabrication of human articular cartilage: a path towards the development of a clinical treatment

RECEIVED
20 March 2018

REVISED
21 July 2018

ACCEPTED FOR PUBLICATION
8 August 2018

PUBLISHED
21 August 2018

Carmine Onofrillo[1,2,3,8], **Serena Duchi**[1,2,3,8], **Cathal D O'Connell**[3], **Romane Blanchard**[1,3], **Andrea J O'Connor**[4], **Mark Scott**[5], **Gordon G Wallace**[2,3], **Peter F M Choong**[1,2,3,6] and **Claudia Di Bella**[1,2,3,6,7]

[1] Department of Surgery, St Vincent's Hospital, University of Melbourne, Clinical Sciences Building, 29 Regent Street, 3065 Fitzroy, VIC, Australia
[2] ARC Centre of Excellence for Electromaterials Science, Intelligent Polymer Research Institute, Innovation Campus, University of Wollongong, NSW, Australia
[3] BioFab3D, Aikenhead Centre for Medical Discovery, St Vincent's Hospital, Melbourne, Australia
[4] Department of Biomedical Engineering, University of Melbourne, Parkville, VIC, Australia
[5] Imaging Laboratory, The Walter and Eliza Hall Institute, 1G Royal Parade, 3052 Parkville, VIC, Australia
[6] Department of Orthopaedics, St Vincent's Hospital, Fitzroy, Victoria, Australia
[7] Author to whom any correspondence should be addressed.
[8] Duchi and Onofrillo contributed equally to this work.

E-mail: carmine.onofrillo@unimelb.edu.au, c.onofrillo@unimelb.edu.au, sduchi@unimelb.edu.au, cathal.d.oconnell@gmail.com, romane.blanchard@unimelb.edu.au, a.oconnor@unimelb.edu.au, scott.m@wehi.edu.au, gwallace@uow.edu.au, pchoong@unimelb.edu.au and claudia.dibella@unimelb.edu.au

Keywords: biofabrication, osteoarthritis, cartilage, stem cells, Biopen, hydrogel, bioscaffold

Supplementary material for this article is available online

Abstract

Cartilage injuries cause pain and loss of function, and if severe may result in osteoarthritis (OA). 3D bioprinting is now a tangible option for the delivery of bioscaffolds capable of regenerating the deficient cartilage tissue. Our team has developed a handheld device, the Biopen, to allow *in situ* additive manufacturing during surgery. Given its ability to extrude in a core/shell manner, the Biopen can preserve cell viability during the biofabrication process, and it is currently the only biofabrication tool tested as a surgical instrument in a sheep model using homologous stem cells. As a necessary step toward the development of a clinically relevant protocol, we aimed to demonstrate that our handheld extrusion device can successfully be used for the biofabrication of human cartilage. Therefore, this study is a required step for the development of a surgical treatment in human patients. In this work we specifically used human adipose derived mesenchymal stem cells (hADSCs), harvested from the infra-patellar fat pad of donor patients affected by OA, to also prove that they can be utilized as the source of cells for the future clinical application. With the Biopen, we generated bioscaffolds made of hADSCs laden in gelatin methacrylate, hyaluronic acid methacrylate and cultured in the presence of chondrogenic stimuli for eight weeks *in vitro*. A comprehensive characterisation including gene and protein expression analyses, immunohistology, confocal microscopy, second harmonic generation, light sheet imaging, atomic force mycroscopy and mechanical unconfined compression demonstrated that our strategy resulted in human hyaline-like cartilage formation. Our *in situ* biofabrication approach represents an innovation with important implications for customizing cartilage repair in patients with cartilage injuries and OA.

1. Introduction

Hyaline cartilage tissue regeneration remains a challenge for musculoskeletal tissue engineering. As a highly specialised tissue, it is characterised by low cell numbers, an avascular, non neural and aliphatic environment, a distinct three-dimensional collagen fibre structure, aggregated proteoglycans and matrix organisation [1]. All these characteristics confer specific mechanical properties [2, 3] and make articular cartilage a challenging tissue to regenerate *in vitro* and *in vivo*. Promising surgical treatments include

Autologous Chondrocyte implantation (ACI) and matrix-induced ACI (MACI) that some have reported to be superior to self-repair inducing techniques such as microfractures [4, 5]. Nevertheless, MACI and ACI are multistage, complex procedures. These techniques require a double operation: the surgical excision of native cartilage tissue and the expansion of adult chondrocytes *in vitro* before implantation [5]. Previous studies have reported that 68% of patients treated with the clinical product approved by the US Food and Drug Administration (Carticel®) had graft failure, delamination or tissue hypertrophy [6]. The major drawbacks include the need for two operations, and that adult chondrocytes have the propensity to undergo de-differentiation [7], thus losing the capability to produce hyaline cartilage extracellular matrix (ECM) and giving rise to reparative tissue that lacks durability [8, 9]. The lack of durability of repaired cartilage leads to the development of osteoarthritis (OA) [10, 11], which severely limits the quality of life of affected individuals and represents one of the greatest contributors to healthcare expenditure worldwide [12].

Regenerating healthy and long lasting articular hyaline-like cartilage is therefore considered a key aim in musculoskeletal tissue engineering [13]. In this regard, mesenchymal stem cells (MSCs) have been heralded as an appropriate candidate for cartilage repair owing to several specific characteristics such as inherent chondrogenic property, ready availability, and cell homing potential [14]. Despite these qualities, their use is still limited, with only 16% of reported cell therapy procedures for cartilage repair registered at https://clinicaltrial.gov/ using MSCs [15].

3D bioprinting has added considerably to standard tissue engineering techniques, thanks to its precision and control [16]. This promising technique can be applied to regenerate biological tissues such as bone and cartilage [17, 18]. A key challenge is now to bring cumbersome bench-based technology to the operating room for real-time application.

3D printing of scaffolds for chondral and osteochondral repair has been tried, using a mosaicplasty-type technique, based on the implantation of scaffolds in defects that are pre-made in the laboratory before surgery [19–22]. 3D printing has the advantage of being coupled with the use of 'custom-designed' implants modelled on pre-operative MRI and/or CT scans. For 'custom designed' bench-based 3D printing techniques a highly detailed pre-operative image of the cartilage defect needs to be obtained, so that the 3D printer can create the desired bioscaffold to match the specific defect. Despite these strategies, however, a mismatch between the bioscaffold and the host defect will likely remain because surgical debridement before implantation alters the anatomy previously imaged, and even the most advanced imaging techniques still fail to identify small gaps and defects. These issues inevitably impede perfectly matching off-the-shelf and custom-designed prefabricated bioscaffolds. The mechanical mismatch between implanted scaffolds and surrounding tissues may inhibit cartilage regeneration at defect sites leading to implant failure [23]. In their literature review, Mollon *et al* summarized the limitations associated with current cartilage repair techniques and noted that graft-site mismatch and size-depth mismatch were the most frequent [24].

To tackle this challenge, we propose *in situ* additive manufacturing as an alternative to computer aided 3D printing. The advantages of *in situ* biofabrication for cartilage regeneration include the possibility of perfectly match the defect geometry without specific preliminary image analysis, shaping the bioscaffold within the defect and achieving the best possible contact between the bioscaffold and the host tissue. *In situ* bioprinting has been proposed as a valid option to deliver at the time and point of need a bioscaffold capable of regenerating deficient tissue [25, 26] and to limit the graft-site mismatch. Also a number of *ex vivo* approaches have been proposed [27, 28] to test the effective use of cell based therapies within a defined defect, but to our knowledge our extrusion device, the Biopen [29], remains the only hydrogel injection system that has been tested as a surgical instrument in a large animal model of cartilage regeneration [30]. The Biopen is an advanced handheld co-axial extrusion device that allows the deposition of cells embedded in a hydrogel material in the surgical setting. Through this device, stem cell laden hydrogel scaffolds can be extruded in a co-axial core/shell distribution, which favourably affects cell survival while maintaining adequate mechanical properties for cartilage tissue engineering purposes. This result is achieved thanks to the segregation of the cells in the core away from the photocrosslinking reaction confined to the shell compartment [31].

Our *in vivo* study was performed using allogenic ovine adipose derived stem cells [30]. To progress towards translating our biofabrication tool into clinical practice, we aim to demonstrate that the advantages of the Biopen are pivotal for the biofabrication of the human cartilage. Therefore, this study is a required step in the development of a clinically relevant protocol for the application of this biofabrication process in the clinical practice (figure 1).

In this study we specifically used human adipose derived mesenchymal stem cells (hADSCs), harvested from the infra-patellar fat pad (IPFP) of donor patients affected by OA, envisioning them as the source of cells for the future clinical application. We screened three different hADSCs from three different patients to take in account also the inter-patient variability. Thus, for each cell line we evaluated stemness and differentiation potential.

We used the Biopen to generate bioscaffolds in which hADSCs were laden in gelatin methacrylate (GelMa) and hyaluronic acid methacrylate (HAMa) [29]. We cultured the bioscaffolds in chondrogenic

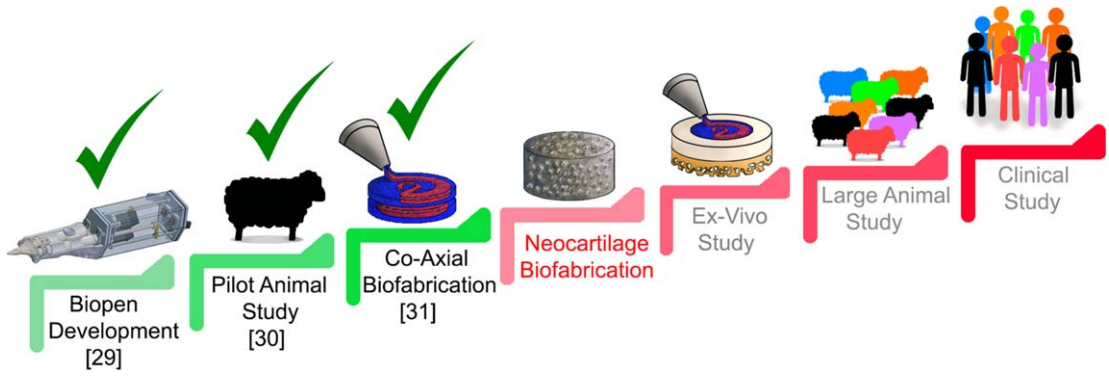

Figure 1. The path towards the development of a clinical treatment. The flow chart lists the steps achieved (in green) and the steps ahead (in red). The current study is indicated as the neocartilage biofabrication step and represents the last *in vitro* analysis before the *ex vivo* and *in vivo* animal studies.

media for eight weeks and we analysed their ability to form hyaline-like cartilage using molecular, imaging and mechanical analyses.

To our knowledge, we are the first to describe the capacity of a surgical device to biofabricate *in situ* a regenerative stem cells niche. The impact of this technology has the potential to change the clinical approaches in the surgical practice for the regeneration of tissues and organs.

2. Materials and methods

2.1. Experimental procedure

Human stem cells were harvested and isolated from the IPFP of patients undergoing total joint knee replacement. A comprehensive profile analysis of immunophenotypic characterization and evaluation of the differentiation potential was used to assess the stemness of three different cell lines from three different donors to be used for the bioprinting step. We then utilized the Biopen to biofabricate the scaffolds. To control the size and shape of our samples, we used PDMS cylindrical moulds of 1 cm diameter and 1 mm thickness with a total volume of approximately 80 μl, so <2 cm^2, which is considered a critical size defect in human cartilage injuries [32]. The limitations of the PDMS material, which is more compliant and flexible than native cartilage, this bioprinting approach guarantees reproducibility of structural organization and cell number, with suitable geometry for mechanical testing, and was used for the entire set of experiments. We then extruded multiple layers until the mould was filled to recreate a 3D structure.

After the photopolymerization reaction, we moved the samples to static culture conditions and we cultivated the samples for 8 weeks in control or chondrogenic differentiation media. The samples, three biological replicates [$n = 3$] for each of the three patients derived cell lines, were collected and analysed every 4 weeks for a total of three time points. We then analysed the capability of our biomanufactoring strategy to produce hyaline-like neocartilage. The cellular response to the chondrogenic stimuli was determined by gene and protein expression analysis. The building of new tissue was defined by protein localization and organization of the main components of hyaline cartilage. The function of the neocartilage was then related to the acquisition of mechanical properties over time (figure 2).

2.2. Synthesis of GelMa/HAMa

Gelatin-methacryloyl/hyaluronic acid methacryloyl (GelMa/HAMa) was synthesized as previously described [31]. Briefly, the materials were dissolved to a final concentration of 100 mg ml^{-1} GelMa and 20 mg ml^{-1} HAMa (10% GelMa-2% HAMa) in sterile PBS (Sigma-Aldrich), containing 100 U ml^{-1} penicillin and 100 μg ml^{-1} of streptomycin (Gibco).

2.3. Stem cells isolation

hADSCs were isolated from human IPFP obtained intraoperatively from total knee arthroplasty with informed consent and approval. Patients with mild/severe OA were recruited. A total of three patients were selected for IPFP harvest. Use of all human samples and procedures in this study was approved by the Human Research Ethics Committee Research Governance Unit of St. Vincent's Hospital, Melbourne, Australia [HREC/16/SVHM/186] and all the experiments were performed in accordance with relevant guidelines and regulations.

hADSCs were isolated and expanded as previously described [33]. Briefly, the fat was diced using a sterile scalpel and digested with 0.1% collagenase type I (Worthington Biochemical) for 3 h at 37 °C under constant agitation, filtered through 100 μm cell strainer nylon (BD Falcon) and centrifuged at 400 g at room temperature for 5 min to separate the stromal fraction from the floating adipocytes. The supernatant was discarded and the cell pellet was resuspended in Red Cell Lysis Buffer (160 mM NH_4Cl; Sigma-

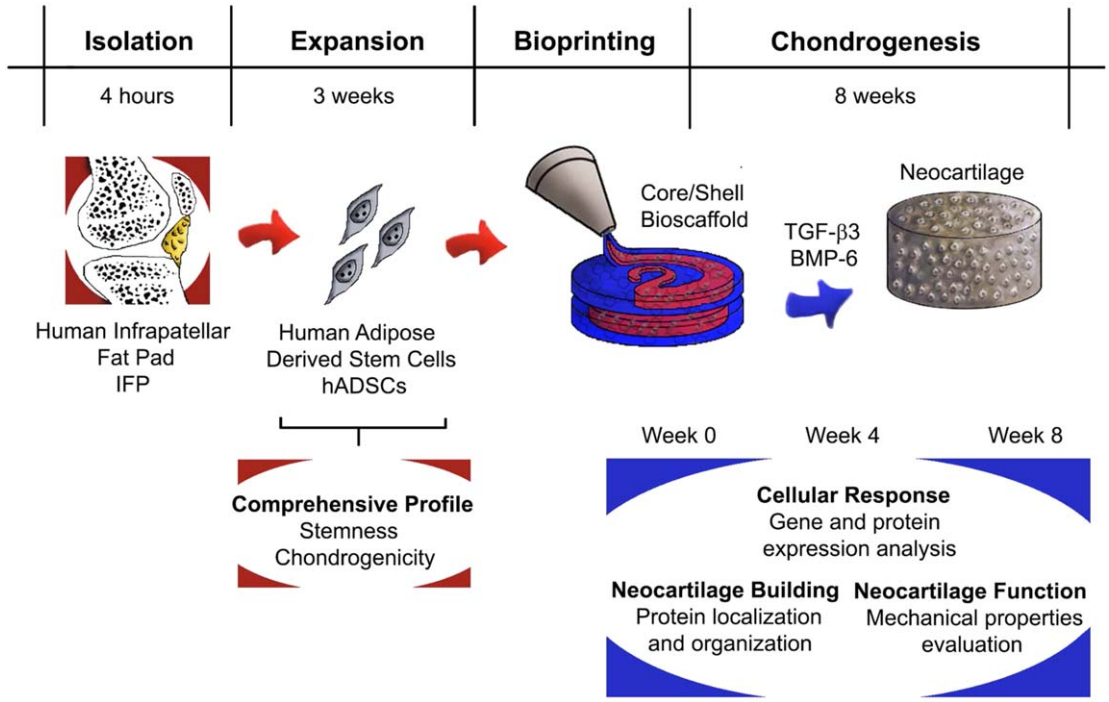

Figure 2. Graphical representation of the experimental procedure and the corresponding time line. Three different cell lines isolated from three patients were analysed in triplicate.

Aldrich) and incubated at room temperature for 10 min. The lysate was centrifuged at 400 g at room temperature for 5 min and filtered through a 40 μm nylon cell strainer (BD Falcon). The isolated cells were then plated in monolayer culture and allowed to adhere for 48 h in culture media containing low glucose DMEM (St. Louis, LA, USA) supplemented with 10% FBS (GIBCO, Thermo Fisher Scientific Inc., Waltham, MA, USA), 100 U ml^{-1} Penicillin and 100 μg ml^{-1} Streptomycin solution (GIBCO), 2 mM L-Glutamine (GIBCO), and 15 mM HEPES (GIBCO), 20 ng ml^{-1} epidermal growth factor and 1 ng ml^{-1} fibroblast growth factor (R&D Systems Inc., Minneapolis, MN, USA). Non-adherent cells were then removed and the medium was replaced with fresh medium. Cells were further cultivated and expanded for cell surface epitope immunophenotypic characterization (flow cytometry) and multilineage differentiation.

2.4. Stemness immunophenotypic characterization and differentiation potential

Immunophenotypic characterization of hADSCs was performed by fluorescence flow cytometry analysis of cell–surface markers at passage 2 (P2). Cells were labelled with monoclonal antibodies against CD14, CD31, CD34, CD45, CD73, CD90, CD106, CD146–FITC conjugates and CD105, HLA-DR, CD29, CD44, CD49e—APC conjugated (Affimetrix eBiosceince, ThermoFisher Scientific). Control samples were labelled with isotype-matched control antibodies IgG1K-FITC and IgG1K-APC (Affimetrix eBiosceince). In brief, cells were trypsinized and aliquoted at a concentration of 2.5 $\times$ 10^5 cells ml^{-1}, fixed in 0.5% paraformaldehyde for 30 min at 4 °C, and washed once in PBS 1X. Next, samples were incubated with either conjugated specific antibodies or isotype-matched control at the manufacturer's recommended concentrations, diluted in PBS 1X supplemented with 5% FBS (FACS buffer). Labelled cells were washed twice, suspended in FACS buffer, and analysed using a FC500 flow cytometer (Beckman Coulter).

Chondrogenic differentiation was induced using the micromass pellet culture technique as described previously [34, 35]. Briefly, 2.5 $\times$ 10^5 confluent P03 cells ml^{-1} were placed in 1.5 ml screw cap tubes (Sarstedt), centrifuged at 400 g for 5 min to form the pellets and cultivated with either non chondrogenic control medium consisting of DMEM high-glucose (Lonza), 100 U ml^{-1} penicillin and 100 μg ml^{-1} of streptomycin (Gibco), 1X Glutamax (Gibco), and 15 mM HEPES (Gibco), or chondrogenic medium consisting of DMEM high-glucose (Lonza), 100 U ml^{-1} penicillin and 100 μg ml^{-1} of streptomycin (Gibco), 1X Glutamax (Gibco), and 15 mM HEPES (Gibco), 1% insulin-transferring-selenium (Sigma-Aldrich), 100 nM dexamethasone (Sigma-Aldrich), 50 mg ml^{-1} ascorbate-2-phosphate (Sigma-Aldrich), 10 ng ml^{-1} TGFβ3 (Prepotech), and 10 ng ml^{-1} BMP6 (R&D Systems).

Osteogenic differentiation was induced at P03 by seeding hADSCs in α-MEM supplemented with 2% FBS in six-well plates at 5 $\times$ 10^5 cells per well. The

next day, an osteogenic inducing cocktail composed of 10 mM β-glycerophosphate (Sigma, St. Louis, MO, USA), 50 μg ml^{-1} ascorbic acid (Sigma) and 100 nM dexamethasone (Sigma) was added.

As a negative control, cells seeded under the same conditions were maintained in a non-inducing medium.

The medium was changed every 2 d and three biological replicates [$n = 3$] per time point and type of analysis at 0 and 4 weeks of culture/group were processed. Immuno/histochemistry and reverse transcription-quantitative polymerase chain reaction (RT-qPCR) were performed as described below.

2.5. Generation of bioscaffolds with the Biopen

Co-axial extrusion was performed using the handheld extrusion system (Biopen) using the same parameters previously described [31]. Briefly, both Biopen chambers were loaded with 10% GelMa-2% HAMa. hADSCs were mixed to a final concentration of 10×10^6 cells ml^{-1} and carefully loaded in the core chamber, while for the shell chamber 0.1% w/v Lithium-acylphosphinate (Tokyo Chemical Industry Co., Tokyo, Japan) was mixed through the GelMa/HAMa. The temperature of the solutions was stabilized at 37 °C prior to preparation. Samples were Biopen extruded into PDMS moulds to produce disc-like shaped bioscaffolds (height = 1 mm, diameter = 10 mm). Immediately after extrusion the samples were then UV irradiated at room temperature for 10 s, using a 365 nm UV source (Omnicure LX400 +, Lumen DynamixLDGI) fitted with a 12 mm lens (25 mm focal distance) with a light intensity of 700 mW cm^{-2}.

2.6. *In vitro* culture of bioscaffolds

The generated bioscaffolds were then transferred to a 24 well plastic plate, washed three times in PBS 1X and 1 ml of chondrogenic or control medium was added to each well. Pictures of the entire samples were taken with a 7 megapixel camera.

Chondrogenic differentiation was induced as previously described for the pelleted culture cells (paragraph 2.3.2.) and three biological replicates [$n = 3$] per time point and type of analysis at 0, 4 and 8 weeks of culture/group (differentiated versus undifferentiated) were processed.

2.7. Histological analysis

For chondrogenic analysis, pelleted cells and Biopen manufactured samples were fixed in 1% paraformaldehyde (Santa Cruz Biotechnology, Dallas, TX, USA) for 4 h at room temperature, embedded in O.C.T. TM Compound (Tissue-Tek, Sakura, Leiden, Netherlands) and flash frozen in liquid nitrogen. Cryosections of 10 μm thickness were mounted onto glass slides and stained with Safranin O (Sigma-Aldrich) for 10 min, dipped in 95% and 100% EtOH, cleared three times for 1 min each in Xylene (Chem-Supply, GILLMAN, SA, Australia) and then mounted in Pertex medium (Grale HDS, Ringwood, VIC, Australia).

For osteogenic differentiation analysis, cultured cells were stained with Alizarin Red-S (AR-S) (Sigma) to reveal the deposition of a calcium-rich mineralized matrix [36]. Quantification of Alizarin was performed by Cetylpyridinium chloride extraction and spectrophotometric measurement at 562 nm.

Samples were imaged using an epifluorescent inverted NikonTiE microscope equipped with a DS-Ri2 and *NIS-Elements* software using a Plan Fluor ELWD 20X DIC L NA 0.45 objective. Figure panels were assembled using Photoshop software (Adobe).

2.8. RNA extraction and RT-qPCR

Total RNA from hADSCs, cultured, pelleted or bioprinted, were harvested at indicated time points using Tri Reagent (Ambion, Austin, TX, USA) according to the manufacturer's protocol. DNA contamination were digested by DNAse I (Sigma). Reverse transcription (RT) was performed using Omniscript RT kit (Quiagen) following the manufacturer's protocol. The relative amounts of COl2A1, COL1A2, ACAN, SOX9, RUNX2, COL10A1, RPL13 and GAPDH RNAs were evaluated with TaqMan Gene expression assay (Applied Biosystems, Foster City, CA, USA) using the following probes:

SOX9 (Hs00165814_m1), ACAN (Hs00153936_m1), COL2A1 (Hs00264051_m1) and COL1A2 (Hs00164004_m1) RUNX2 (Hs01047973_m1), COL10A1 (Hs00166657_m1) as target genes; GAPDH (Hs02786624_g1) and RPL13a (Hs04194366_g1) as housekeeping genes. qPCR was performed on a QuantStudio 6 Flex Real-Time PCR System (Thermo Fisher Scientific) and relative quantification was calculated with the 2E−ΔΔCT method. The mean ΔCT value of the control sample was used in each experiment to calculate the ΔΔCT value of sample replicates by using an average of two different housekeeping genes (RPL13 and GAPDH). Statistical analysis on the data obtained was performed by using unpaired *T*-Test on three experimental replicates by considering significative data with a P *value* < 0.05. Graphs were designed using Prism 5 software (GraphPad) and figure panels were assembled using Photoshop software (Adobe).

2.9. Protein extraction and Western blot analysis

Biopen printed samples were collected at the indicated time points, washed three times for 5 min each with PBS 1X on a rotating platform at room temperature, transferred in a 1.5 ml Eppendorf tube, then flash frozen in liquid Nitrogen and stored at −80°C. Whole protein content was extracted on ice by manually break with a pestle in 30 μl/samples of 2X RIPA buffer (750 mM NaCl, 5% Triton X100; 2.5% Sodium Deoxycolate; 10% SDS; 1M Tris, pH 8) with the

addition of protease inhibitor cocktail (Roche). Samples were incubated on ice for 20 min and cleared by centrifugation at 14 000 rcf for 20 min at 4 °C. The supernatant was recovered and carefully transferred in a new labelled tubes. Protein extract was quantified spectrophotometrically with the BCA Protein Assay (Thermo scientific). The same amount of proteins was separated in loading buffer (Thermo scientific) in 4%–12% Bolt Bis-Tris precast Gel (Thermo scientific) in MES buffer (Life technologies) for 30 min at constant voltage (180 V). Spectra Multicolor Broad range protein ladder (Thermo scientific) was used as a protein standard. After the electrophoretic separation, proteins were blotted to PVDF membrane with iBlot 2 system (Life Technologies), following manufacturer's instructions. Protein transfer was assessed by Ponceau (sigma) staining. The membrane was blocked against non specific bindings with 5% non-fat dry milk (Coles) in TBS-T (50 mM Tris-Cl, pH 7.6; 150 mM NaCl; 0.1% Tween 20) for 1 h at room temperature. After three washes in TBS-T for 10 min, the membrane was incubated overnight at 4 °C with rabbit monoclonal anti human SOX 9 antibody (#EPR14335, Abcam) or mouse monoclonal anti human β-Actin (#A5316, Sigma-Aldrich) in 3.5% Bovine Serum Albumin in TBS-T. After three washes in TBS-T for 10 min, the membrane was incubated for 1 h at room temperature with anti-rabbit secondary antibody HRP conjugated (Dako). Finally, after three washes in TBS-T for 10 min, the signal was revealed with Western Blot Lightning ECL pro kit (PerkinElmer) and imaged with Chemidoc MP imaging system (Biorad). Figure panels were assembled using Photoshop software (Adobe).

2.10. Immunostaining analyses and fluorescent imaging

For fluorescence analysis, 10 μm thickness slices from both pelleted cell culture and Biopen printed, were washed three times in PBS1X and permeabilized for 15 min in PBS 1X-0.1% TritonX-100 (PBT). Antigen retrieval was performed only for hydrogel printed samples by adding 1 mg ml^{-1} Hyaluronidase (SIGMA, #H6254) diluted in PBS 1X and incubating 30 min at room temperature. After three washes 5 min each in PBS 1X, samples were dropped in blocking solution (10% goat serum diluted in PBT) for 60 min at room temperature and then incubated overnight at 4 °C with mouse anti-human Collagen II (#II6B3, DSHB), goat anti-human Collagen I (#sc8784, Santa Cruz), mouse anti-human Proteoglycan (#MAB2015, MerckMillipore) and mouse anti-human Collagen X (#ab49945, Abcam), diluted 1:250 in blocking solution. The day after, samples were washed three times for 10 min each and secondary antibodies both diluted 1:100 in blocking solution were added, respectively anti-mouse IgG Alexa Fluor-647 (#715-605-151, Jackson Immuno Research) and anti-goat IgG Alexa Fluor-546 (#A11056, Thermo Fisher Scientific Inc.), and incubated for 2 h at room temperature. After three washes 5 min each in PBS 1X, actin was labelled with Texas Red-X Phalloidin (#T7471, Thermo Fisher Scientific Inc.) 1:100 diluted in PBS 1X for 60 min at room temperature and nuclei were stained by incubation with 5 μg ml^{-1} DAPI (Thermo Fisher Scientific Inc.) diluted in PBS 1X for extra 60 min at room temperature.

The sections were washed three times 5 min each in PBS 1X, mounted with Fluoromount-G (Southern Biotech, Birmingham, AL, USA) onto glass slides. Pellet sections were imaged using an epifluorescent inverted NikonTiE microscope equipped with a DS-Ri2 and *NIS-Elements* software using a Plan Fluor ELWD 20X DIC L NA 0.45 objective. Biopen printed samples were imaged with NikonA1R confocal microscope using a Nikon Plan

VC 20× DIC N2 N.A. 0.75 objective lens and 'Scan large image' from *NIS-Elements* software tool was used to image a larger field of view.

Digital images were processed using *NIS-Elements* software (Nikon, Amsterdam, Netherlands) and Photoshop software (Adobe) was used to assemble the figure panels. All the images shown in this study are representative of at least three independent experiments.

The fluorescence measurement analysis of figure 6(C) was performed with the 'Annotations and Measurements' feature of *NIS-Element* software.

The intensity of the Collagen type II corresponding channel was calculated by normalizing the signal for the identified positive area. The percentage of the positive area was calculated in relation to the total area of the field of view, which was the same for all the images acquired and that corresponded to 3 mm^2.

Those analyses were performed on three different fields of view for each sample.

2.11. Second harmonic generation (SHG) microscopy

Regions of interest images (5 mm × 5 mm) were acquired on a fully automated, programmable, multiphoton imaging platform (Genesis® 200, HistoIndex Pte Ltd, Singapore) following sectioning and mounting of 10 μm thick cryosections washed out from OCT. Laser excitation occurred at 780 nm. Forward-scatter two-photon excitation (TPE) and SHG signals were detected using dedicated photomultiplier tubes for each channel. Magnification was set to 20×. TPE sensitivity was set to 0.7, and SHG sensitivity to 0.6. A bandpass filter with center wavelength at 550 nm and bandwidth of 88 nm was set in front of the TPE photodetector. Laser baseline power was set at 0.5, and then stepped down by 60% using a set of 2 optical attenuators (0.1OD, 0.3OD—'Low' laser power configuration). No change was made to the polarization of the laser source, and no polarization was used on the

SHG detection channel. Tissue areas were scanned once with no frame averaging feature.

2.12. Whole sample staining and light sheet imaging

Entire bioscaffolds were transferred to clean 12 well plates, washed 3 times 10 min each in PBS 1X and fixed in Paraformaldehyde 4% for 30 min. After washing three times for 10 min each in PBS 1X, samples were permeabilized in PBT (0.1% Triton in PBS 1X) for 60 min. Actin was labeled with Texas Red-X phalloidin (#T7471, Thermo Fisher Scientific Inc.) 1:100 diluted in PBS for 2 h. The excess of phalloidin was removed by washing 3 times 10 min each in PBS 1X. Nuclei were stained by incubation with 5 μg ml^{-1} DAPI (Thermo Fisher Scientific Inc.) diluted in PBS 1X for extra 60 min. Samples were finally washed 3 times 10 min each in PBS1X and left at 4 °C until imaging.

For light sheet imaging, samples were hooked and loaded in a glass capillary (size 2 black, inner diameter of capillary ~1 mm, #701932, BRAND GmbH). The glass capillary was mounted in the chamber, which was filled PBS 1X. A Lightsheet Z.1 microscope (Carl Zeiss Microscopy GmbH, Jena, Germany), with 20×/1.0 NA water dipping detection objective and two-sided 10×/0.2 illumination optics, equipped with two PCO EDGE 4.2 cameras (sCMOS sensor, square pixels of 6.5 × 6.5 μm side length, 2048 × 2048 pixel resolution, 3-channel images, 16 bit dynamic range) (PCO AG, Kelheim, Germany) were used for light sheet imaging. For DAPI and Phalloidin-actin 1.5%–405 nm and 8.6%–561 nm laser powers respectively and 50 ms exposure time were used. Pivot scanning mode (Carl Zeiss) was used to deliver homogeneous illumination and prevent shadows along the illumination axis. For all 3D datasets, a z-interval of 2 μm with a zoom of 0.50 was used. The volumetric images were 1131 × 1131 × 1000 μm (1920 × 1920 × 500 pixels) in size, with 0.589 × 0.589 × 2.000 μm^3 resolution. To counteract the degradation of the light sheet by the high amount of scattering, the specimen was sequentially illuminated through each of the two opposing illumination objectives, generating pairs of illuminated single-side images, and then combined into fused single illumination optical sections with a considerably improved penetration depth. All acquired LSFM raw data were processed using ZEN 2011 imaging software (Carl Zeiss, Germany). Optical sections were merged and combined into a single three-dimensional data set and reconstructed using IMARIS 9.0 software.

2.13. Compression testing

The tests were performed at room temperature using a TA Electroforce 5500 mechanical loading device (TA Instruments, New Castle, USA) fitted with a calibrated 22 N load cell. The contact point between the two plates was recorded. Then, the sample was placed between two 4.2 cm diameter compression plates, in an unconfined setting as previously described [37]. The displacement of the upper plate was controlled by a ramp function, at a rate of 0.01 mm s^{-1}, until a total displacement of 25% of the sample height. The contact area of the sample with the plate was measured by microscopy imaging before the test. Additionally, the point of inflexion of the load versus time curve showed the contact point between the sample surface and the compression plate to give the sample height. Load and displacement measurements were converted into stress (σ) and strain (ε) data using the sample surface area and height. The compressive modulus was then computed using stress data between 10% and 15% strain as follows: $E_c = (\sigma_{15} - \sigma_{10})/(\varepsilon_{15} - \varepsilon_{10})$. Three biological replicates [$n = 3$] for each of the three patients per time point and type of analysis at 0, 4 and 8 weeks of culture/group (differentiated versus undifferentiated) were processed. Data graphs were designed using Prism 5 software (GraphPad).

2.14. Atomic force microscopy

AFM nanoindentation was performed on an MFP-3D (Asylum Research) using a contact mode MLCT probe (Bruker Nano Inc.) with a stiffness calibrated as 0.135 N m^{-1}. Force curves were performed to an indentation force of 5 nN at an approach rate of 2 m s^{-1}. The Young's Modulus was obtained using the Hertz indentation model approximating the tip-shape as a 19.2° cone. Bioprinted hydrogel samples were submerged in PBS 1X during measurement.

Sixteen indentations across 5 regions were performed in astandardized fashion, making 80 force curves per sample. Three samples for each of the control week 8 and chondrogenic week 8 groups were measured. The same AFM probe was used for all measurements.

2.15. Statistical analysis

All statistical analyses were performed using Prism 5 (GraphPad) software. Differences between the experimental groups were determined using unpaired t test or one-way Anova tests with Dunnett's corrections as indicated. Significance was represented as follow:

$^{*} = p \leqslant 0.05$; $^{**} = p \leqslant 0.01$; $^{***} = p \leqslant 0.001$; not significant (n.s.) $= p > 0.05$.

3. Results

3.1. Comprehensive profile analysis of hADSCs identifies the IPFP as a source of stem cells for *in situ* biofabrication

In order to account for any possible inter-patient variability, we decided to test our biofabrication strategy on different stem cells lines derived from three donors. Thus, we isolated infra-patellar hADSCs from three patients undergoing total joint knee replacement and characterized their stemness and differentiation potential.

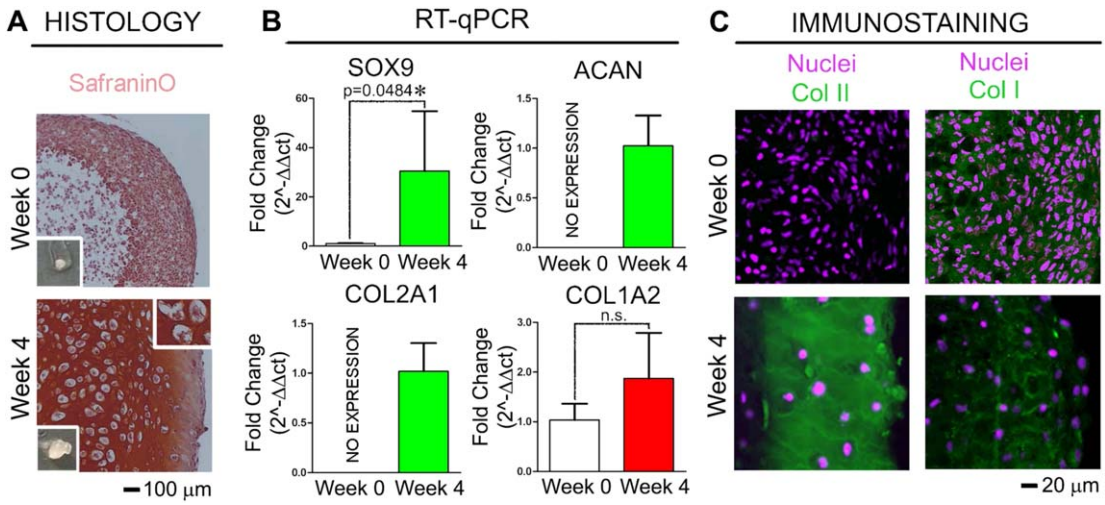

Figure 3. Comprehensive profile analysis of infrapatellar fat pad derived hADSCs. (A) Histological analysis on 10 μm cryosections stained with Safranin O to detect accumulation of GAG in the ECM. In the bottom left, the insets show the brightfield images of the whole pellets. The small panel on the right upper corner at week 4 shows a higher magnification image of cells encapsulated and surrounded by the ECM. (B) The graphs represent the fold changes calculated with 2^ΔΔCT method of Collagen type II (COL2A1) and type I (COL1A2), Aggrecan (ACAN) and Sox-9 (SOX9) markers. Fold Changes were normalized for RPL13a and GAPDH. Error bars represents standard deviation between three biological replicates and significant activity was calculated with unpaired t-test. These analyses have been performed on the hADSCs lines derived from three different patients and statistical analyses were performed as described in Materials and methods section. (C) Immunostaining analysis on 10 μm cryosections from pellet at weeks 0 and 4 of chondrogenesis, performed using antibodies against Collagen type II (Col II) and I (Col I) shown in green, and DAPI shown in violet to detect cells nuclei. Note: the images in A and C are the most representative selected from the immunohistology performed on the three hADSCs patient derived cell lines.

We first evaluated the cell morphology, plastic adherence after isolation and expression of typical stemness surface markers. The three lines displayed the typical spindle-shaped appearance at early passages and exhibited a smoothened morphology after long-term expansion, developing a larger and more granular cytoplasm (data not shown). Flow cytometry analysis documented that >90% of hADSCs expressed CD90, CD73, CD105 CD29, CD49. More than 90% of cells were also positive to the hyaluronan receptor CD44, which role is important in the early stages of cartilage development [38]. More than 60% of hADSCs were positive for HLA-DR, whereas the expression of the hematopoietic markers CD14, CD31, CD34, CD45 was <3%. The markers CD106 and CD146 were expressed in less than 10% of hADSCs as previously shown [39]. No significant difference among the three patients was scored, confirming that with our established laboratory procedures we are able to isolate and expand a homogenous stem cell population despite the donor tissue variability (supplementary figure 1 is available online at stacks.iop.org/BF/10/045006/mmedia). The chondrogenic potential was then tested by pellet culture *in vitro* during a period of 4 weeks, and production of chondral ECM was confirmed (figure 3).

The initial assessment of chondrogenesis was based on the size and appearance of the pellets. After their generation, pellets grew in size and displayed a consistent white opaque macroscopic appearance (figure 3(A)). Safranin O staining showed accumulation of glycosaminoglycans (GAGs) deposition (figure 3(A)) and changes in cell morphology from round shapes at week 0 to elongated cells encapsulated by an abundant ECM in the entire pellet structure (figure 3(A)). Gene expression data confirm the increase expression of Collagen type II (COL2A1) and type I (COL1A2), Aggrecan (ACAN) and Sox-9 (SOX9) markers during the differentiation process (figure 3(B)). COL2A1 and ACAN were not detectable in both 2D and pellet cultured hADSCs at steady state, but were activated only during the chondrogenesis process as a consequence of SOX9 increased expression. Finally, the immunostaining analyses revealed an increased expression of both Collagen type II and I during time, with a much stronger intercellular accumulation of Col II (figure 3(C)). As previously shown [34, 35], hADSCs from fat pad display the tendency to express higher level of collagen type II RNA and protein respect to Collagen type I during *in vitro* chondrogenesis under stimulation of TGFβ3 and BMP6.

To confirm further the differentiation potential of the isolated populations, we also tested the osteogenic potential through Alizarin red staining and gene expression (supp. figure 2).

3.2. Neocartilage generation *in vitro*

3.2.1. GAG accumulation during chondrogenic differentiation of hADASCs in GelMa/HAMa bioscaffolds

We used the Biopen to generate bioscaffolds in which hADSCs were laden in GelMa and HAMa. Both Gelatin (denatured collagen) and hyaluronic acid retain relevant cell-binding sites, while the addition of

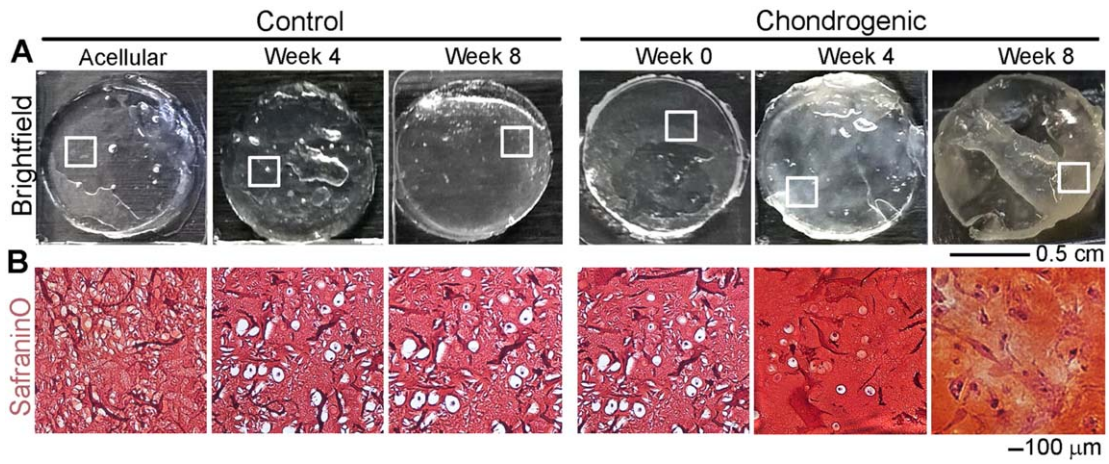

Figure 4. Neocartilage building and evaluation of GAG accumulation in Biopen extruded bioscaffolds. (A) Photographs show bioscaffolds from the control and the chondrogenic groups at the indicated time points. The white boxes outline the areas imaged in the histological analysis shown in the corresponding panels below. (B) Histological analysis from the corresponding samples of 10 μm cryosections, stained with Safranin O dye. Images were acquired with a 20× objective lens. Note: the images in A and B are the most representative selected from the analyses performed on bioscaffold constituted by three hADSCs lines derived from three different patients.

methacrylate groups renders the material amenable to rapid crosslinking using light, creating a hydrogel structure which is stable at physiological temperatures and achieves mechanical properties approaching that of native hyaline cartilage. As described in our previous paper [31] the 10 s crosslinking time at 700 mW cm^{-2} with a 365 nm UV light source do not cause proliferation inhibition to hADSCs in the same core/shell bioprinting conditions.

We produced tridimensional structures of the size of a critical cartilage injury, where a critical size implies a defect which will not heal spontaneously without any intervention [40, 41].

The neocartilage development was first qualitatively evaluated via the appearance of the bioscaffolds. The macroscopic brightfield images showed a marked difference in the opacity of the printed samples with a consistent white opaque macroscopic appearance developing over time only in the chondrogenic stimulated samples and not in the control group (figure 4(A)).

The deposition of the ECM in the hydrogel matrix was then verified histologically, by staining the sections derived from the same samples with Safranin O, as a reporter of GAG content [42] (figure 4(B)). In the acellular scaffold, Safranin O stains a non-homogenous material. On the other hand, in the cell–laden bioscaffolds, the stem cells occupied defined lacunae in the surrounding hydrogel and exhibited a round shaped morphology when maintained in a control non-chondrogenic media.

Upon chondrogenesis, the bioscaffolds showed a progressive formation of a compact and homogeneous matrix at weeks 4 and 8 that is positive to Safranin O, demonstrating the accumulation of GAG (figure 4(B)). The cells appeared elongated throughout the GAG forming a continuous structure. This analysis indicated a cell response to chondrogenic stimuli in GelMa/HAMa bioscaffolds and the consequent accumulation of GAG over time.

3.2.2. Gene expression analysis evidences chondrogenic differentiation of hADSCs in GelMa/HAMa bioscaffolds

To elucidate the capability of hADSCs to undergo chondrogenesis in the bioscaffolds, we analysed the gene expression of chondrogenic markers over a period of 8 weeks by RT-qPCR and Western blot analyses.

The three hADSCs lines showed a progressive increase of the master transcriptional regulator of the chondrogenic program SOX9 both at transcriptional and translational level [43, 44] (figures 5(A), (B)).

The intracellular accumulation of SOX9 led in turn to a progressive activation of its target genes COL2A1 and ACAN (figure 5(A)). The three hADSCs lines did not exert any basal expression of the ECM components before the induction of chondrogenesis, as also confirmed by electrophoretic analysis of PCR amplified cDNA (figure 5(A), lower panels). ACAN and COL2A1 expression was detectable 4 weeks after the start of the chondrogenesis differentiation, exerting an average fold change of 20 and of 140 respectively during the following 4 weeks. hADSCs already expressed COL1A2 before the chondrogenesis differentiation and its level increase during time. Nevertheless, COL1A2 showed only a 10 fold increase from week 0, while Collagen type II, which was not detectable at week 0, increases up to 200 folds at week 8 compared to week 4. Thus, the ratio between COL2A1 and COL1A2 indicated the generation of hyaline-like cartilage rather than fibrocartilage, as described in previous works [45, 46] and in agreement with pellet culture data (figure 3).

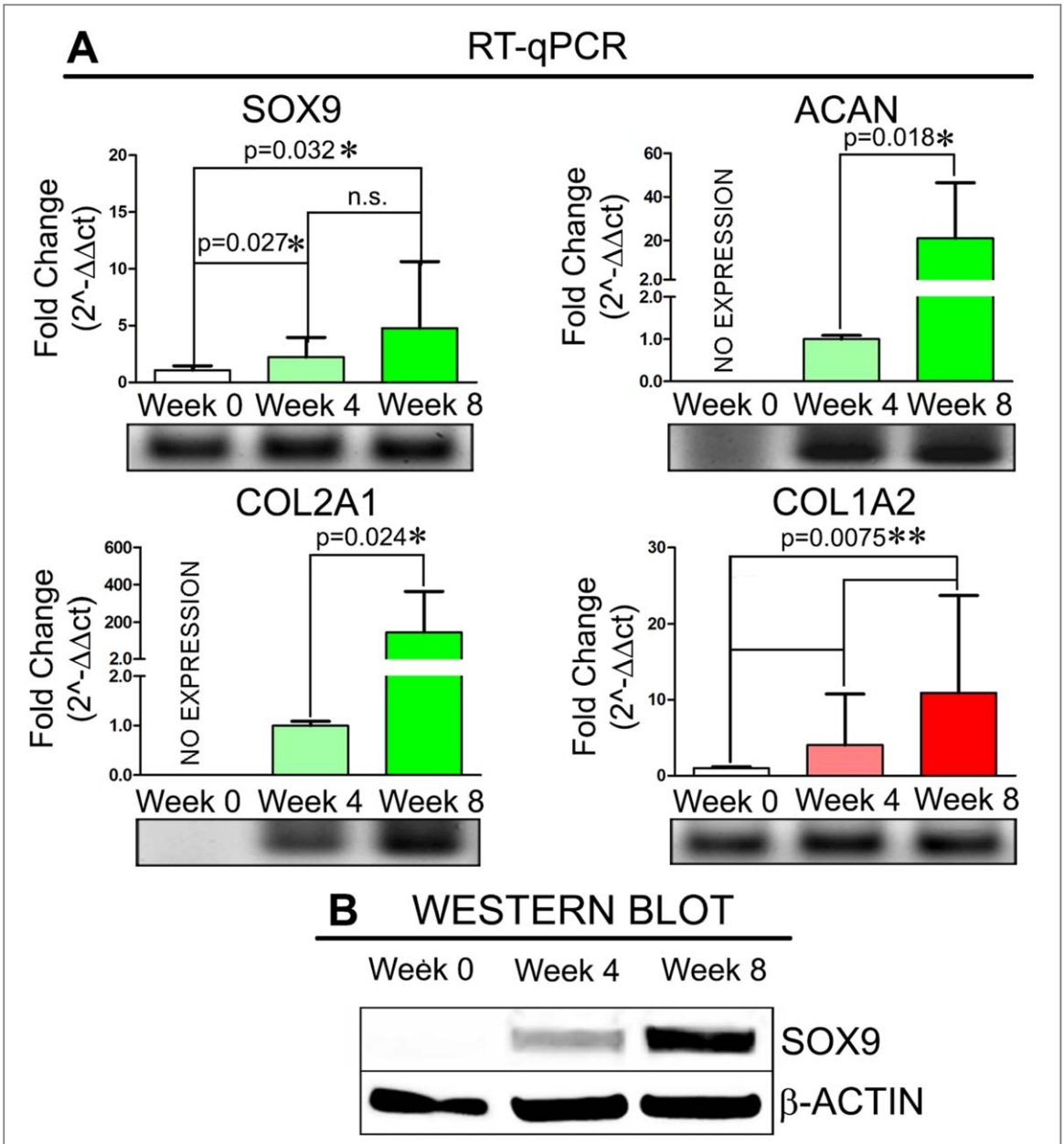

Figure 5. Cellular response to chondrogenic stimuli. (A) The graphs represent the fold changes calculated with the 2^ΔΔCT method of Collagen type II (COL2A1) and type I (COL1A2), Aggrecan (ACAN) and Sox-9 (SOX9) markers. Fold changes were normalized for RPL13a and GAPDH. Error bars represents standard deviation between three biological replicates and significativity was calculated with unpaired t-test. These analyses have been performed on lines derived from three different patients. The lower panels show the electrophoretic analysis of the amplified cDNA to underline the switch in COL2A1 and ACAN expression during chondrogenesis. (B) Western blot analysis of SOX9 protein expression in hADASCs undergoing chondrogenesis in GelMa/HAMa bioscaffolds.

3.2.3. Generation of hyaline-like cartilage

To analyse the process of biofabrication of chondral tissue in our Biopen extruded samples, we cryosectioned the bioscaffolds at the indicated time points and performed histological analysis by immunostaining with antibodies against Collagen type II (Col II), Collagen type I (Col I) (figure 6) and Proteoglycan (supp. figure 3). The data obtained matched the gene expression analysis: Col I was already expressed at the start of the chondrogenic differentiation, while Col II was detected after 4 weeks (figure 6(A)).

Despite the fact that the intensity of the Col I signal increased during chondrogenesis, the intercellular Col II deposition and accumulation in the hydrogel matrix dramatically differed from Col I, reaching a strong and uniform pattern at week 8 of chondrogenesis. The thickness of the Col II-rich stripe increased from an average length of 400 μm at week 4 up to 800 μm at week 8 (figure 6(A)). Those data are consistent with RT-PCR expression analyses where we demonstrated that the ratio between Collagen II and I is in favor of Collagen type II higher expression. Those results correlates with the generation of hyaline-like neocartilage.

To confirm these data we analysed the fluorescence intensity profile and the relative percentage of the area that was positive for Col II on three fields of view for each of the three patient derived cell lines

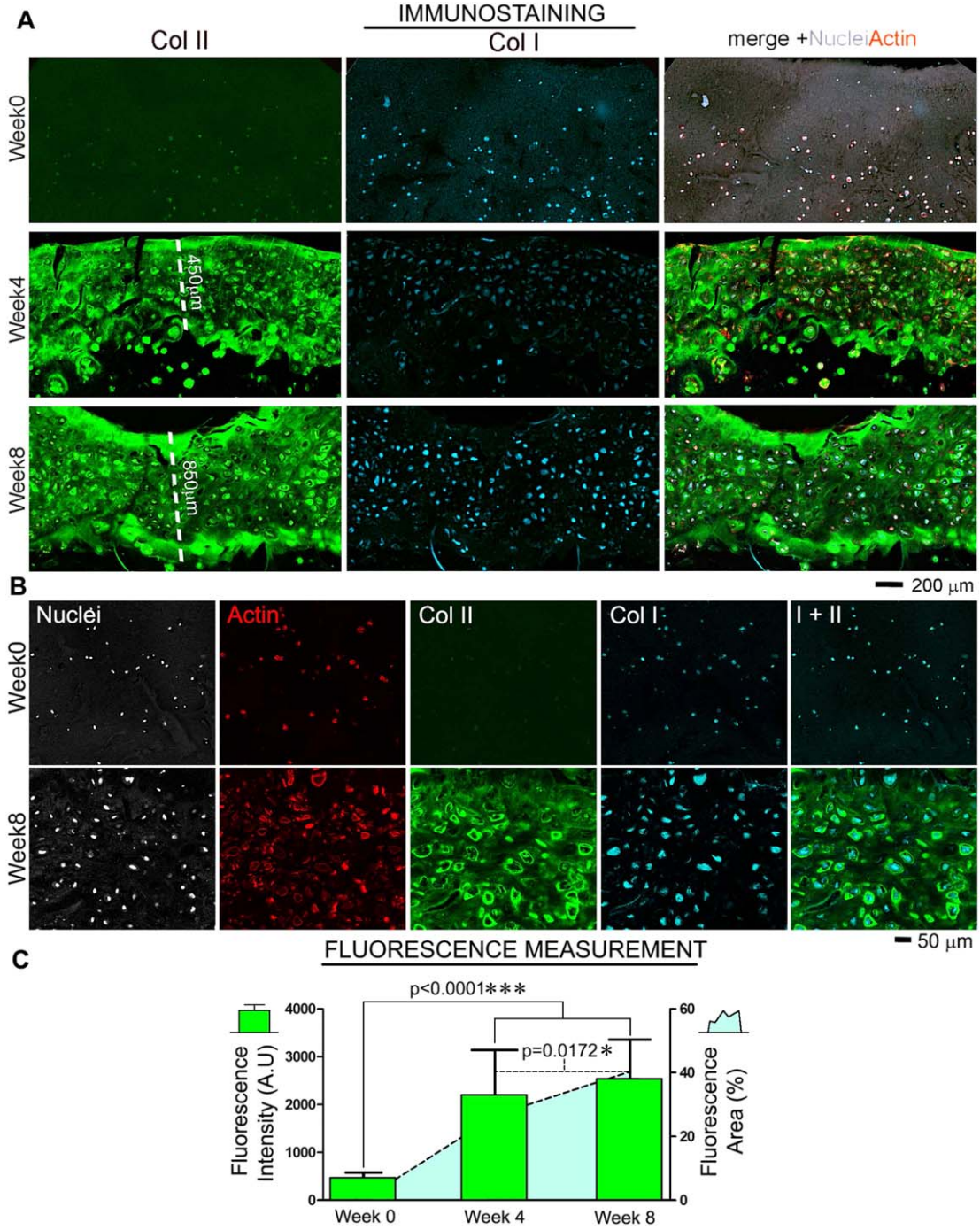

Figure 6. Neocartilage building and accumulation of Collagen type II. (A) Immunostaining analysis on 10 μm cryosections from Biopen biofabricated samples at weeks 0, 4 and 8 of chondrogenesis, performed using antibodies against Collagen type II (Col II, in green), Collagen Type I (Col I, in cyan) and counterstained with cell marker nuclei DAPI (in grey) and Texas Red-X phalloidin Actin (in red) to detect cell morphology. The superimposed signals are shown in the last columns (merge + Nuclei Actin). The images are orientated with the surface of the samples toward the top. (B) The panels show higher magnification of sections shown in A. Note: the images are the most representative selected from the immunohistology performed on the three hADSCs patient derived cell lines. (C) The graph shows the quantification analysis of Col II fluorescence intensity (in panel A) normalized for the positive area (bars) and the percentage of the positive area for Col II (area fill). The calculations were performed on three different fields of view. One way Anova with Dunnett's correction was applied to statistically analyse the differences in the fluorescence intensity, while unpaired t test was used for the fluorescence area.

(figure 6(B)). The results showed a significant difference in the fluorescence intensity between the samples collected at the start of the chondrogenesis and the differentiated samples at weeks 4 and 8 on an area of 3 mm^2 for each field analysed. Moreover, the fluorescent area was 26% of the 3 mm^2 area at week 4 with a significant increase up to 40% at week 8 (figure 6(C)). The changes in cell morphology during differentiation represents an important feature to estimate the degree of chondrogenesis [47]. As detected by actin staining of cytoskeleton, hADSCs modified their morphology over time from round shape to a more elongated

appearance (figure 6(B)). Collagen type II was strongly concentrated along the cell's membranes and in the ECM, while collagen type I remained confined in the intracellular area (figure 6(B)). Moreover, Collagen type X, a marker of hypertrophic differentiation, resulted to be expressed after 4 weeks of chondrogenesis, also with an intracellular accumulation (supp. figure 4).

Conversely, in the control bioscaffolds, in absence of chondrogenic stimuli, the expression of Collagen type I and II was not detectable (supp. figure 5).

In order to visualize the spatial distribution of cells and ECM deposition along the differentiation, we used Light Sheet microscopy, which allows the reconstruction of a 3D image, while maintaining the physiological integrity of the bioscaffold through optical sectioning of the sample. We labelled the bioscaffolds with Actin to detect cells and with Collagen type II to detect ECM generation. From our imaging analysis, we observed how hADSCs exerted the ability to condense in the GelMa/HAMa hydrogel scaffold during the chondrogenesis (figure 7). Cells are evenly distributed along the entire depth of the printed scaffold right after the printing (figures 7(A), (C)), but condensed toward the superficial areas of the bioscaffolds during the chondrogenic differentiation (figures 7(B), (D)). In contrast, the condensation phenomenon was not visible without chondrogenic stimuli (supp. figure 4). Collagen type II deposition is clearly visible at week 4 in the area where cells are condensed. The stem cell condensation is in fact required for the inception of the chondrogenic program during limb development [48, 49].

3.2.4. Collagen II fibrillary organization in GelMa/HAMa bioscaffolds

Visualization of the 3D arrangement of the ECM and living cells in native hydrated conditions is crucial to ensure the formation of a hyaline-like tissue [49]. In addition, it is important to understand if the accumulation of Collagen type II is combined with the organization of mature collagen fibrils that provides the strength and the function to the neotissue.

Hence, the immunohistochemistry analysis was complemented with nonlinear microscopy, a non-invasive methodology that allows to simultaneously acquire SHG images of collagen and TPE autofluorescence images of living cells in label-free biofabricated scaffolds (figure 8(A)).

In the acellular scaffolds that were maintained in chondrogenic media for 8 weeks, TPE and SHG were not detectable, indicating that the composition of GelMa/HAMa did not interfere with the two signals' generation (figure 8(B)). In the chondrogenic induced bioscaffolds, we were able to detect TPE signals from cells embedded in the GelMa/HAMa and SHG derived image of collagen fibrils surrounding the cells (figure 8(D)). In contrast, in absence of chondrogenic stimuli, only TPE signal was detectable (figure 8(C). The collagen-like fibrils detected by SHG are only attributable to the building of neocartilage from stem cells undergoing chondrogenesis. Importantly, given that the corresponding immunostaining performed on the same sections was able to detect only Collagen type II protein accumulation in the ECM, rather than Collagen type I or Collagen type X (figure 6 and supp. figure 3), mature Collagen type II can be considered as a major contributor of the SHG signal.

3.2.5. Mechanical evaluation of GelMa/HAMa bioscaffolds during chondrogenesis

In order to characterize the functional development of the *in vitro* generated tissue, we used unconfined compression testing (figure 9) on the three hADSCs cell lines in triplicate for each indicated time point. The unconfined compressive modulus measured in non chondrogenic bioscaffolds was 57.28 kPa (+/−26.8) and 29.9 kPa (+/−23.4) after 8 weeks of chondrogenesis without any significative difference between the groups (figure 9(A)).

Moreover, the bioscaffolds exerted a compressive modulus of 61.2 (+/−36.5) at week 0 (data not shown). Overall, we measured that the bioscaffolds maintain consistent mechanical properties along the chondrogenic differentiation. However, by analysing the surface of our bioscaffolds at a microscale level by atomic force microscopy indentation, we found that the Young's modulus of five different localized area of three different samples was 660 kPa (+/−1119) after 8 weeks of chondrogenesis and only 191.7 kPa (+/−140.7) in their relative non chondrogenic controls. The high variability of the chondrogenic samples reflects the accumulation of biological derived ECM, for which organization is based on collagen fibrils and cannot result in a flat homogeneous surface. The stiffness is on average 3.45 times higher than their control counterparts, which in contrast showed a much lower standard deviation (figure 9(B)).

Thus, the secreted matrix causes a gain in mechanical strength that cannot be detected by unconfined mechanical tests due to the non-homogeneous organization of the neocartilage through the entire thickness of the sample.

4. Discussion

The results of this study demonstrate that the Biopen can be used to produce human hyaline-like cartilage *in vitro* by co-axial extrusion of hADSCs laden in GelMa/HAMa hydrogel.

The necessity for the development of a handheld device is dictated by surgical needs: cartilage injuries have to be cleaned and debrided before any regenerative solution can be attempted surgically, therefore impeding the perfect matching of laboratory-produced bioscaffolds.

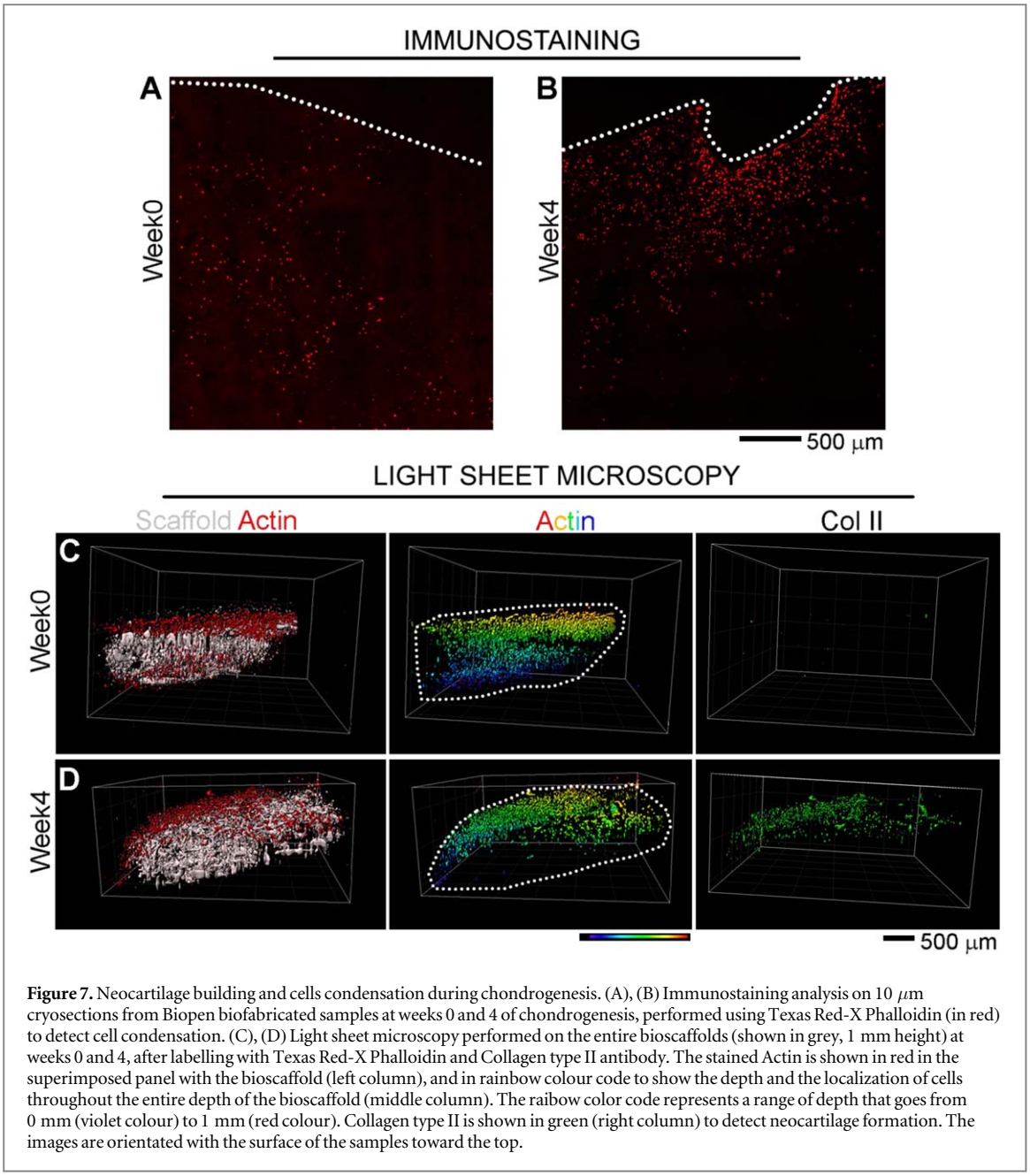

Figure 7. Neocartilage building and cells condensation during chondrogenesis. (A), (B) Immunostaining analysis on 10 μm cryosections from Biopen biofabricated samples at weeks 0 and 4 of chondrogenesis, performed using Texas Red-X Phalloidin (in red) to detect cell condensation. (C), (D) Light sheet microscopy performed on the entire bioscaffolds (shown in grey, 1 mm height) at weeks 0 and 4, after labelling with Texas Red-X Phalloidin and Collagen type II antibody. The stained Actin is shown in red in the superimposed panel with the bioscaffold (left column), and in rainbow colour code to show the depth and the localization of cells throughout the entire depth of the bioscaffold (middle column). The raibow color code represents a range of depth that goes from 0 mm (violet colour) to 1 mm (red colour). Collagen type II is shown in green (right column) to detect neocartilage formation. The images are orientated with the surface of the samples toward the top.

In this study, we have used the handheld extrusion device (Biopen) in the same fashion as it would be used surgically, to simulate its clinical applicability.

The ideal cell type to be used for cartilage regeneration is still a matter of debate. A number of cell sources have been investigated, the most common being mature articular chondrocytes, chondrocyte progenitors, and stem cells [50]. It is accepted that overall MSCs must possess a proven chondrogenic capacity, must not cause donor-site morbidity, and must be readily expandable in culture without losing their phenotype [51]. The number of stem cells-based clinical trials currently running worldwide and focused on cartilage repair is in fact increasing [52]. Recently, a group of stem cells isolated from joint tissue, such as chondrogenic stem/progenitors from cartilage itself, synovial fluid, synovial membrane, and IPFP have gained great attention due to their increased chondrogenic capacity over the bone marrow and subcutaneous adipose-derived stem cells [53]. Indeed, the IPFP, has gained much attention as a source of hADSCs with high chondrogenic capacity both *in vitro* and in tissue regenerative medicine approaches [53]. Human ADSCs also express CD44, which is the hyaluronic acid receptor involved in cell–cell and cell–matrix interactions, therefore playing an important role in the early stages of cartilage regeneration [38]. By expressing CD44, these cells are more prone to bind the hyaluronic acid residues present in the GelMa/HAMa bioink favouring the chondrogenic process. Therefore, for our study we have selected hADSCs harvested from the IPFP, as the source for human cartilage regeneration. Furthermore, we have shown that stem cells isolated from the IPFP of

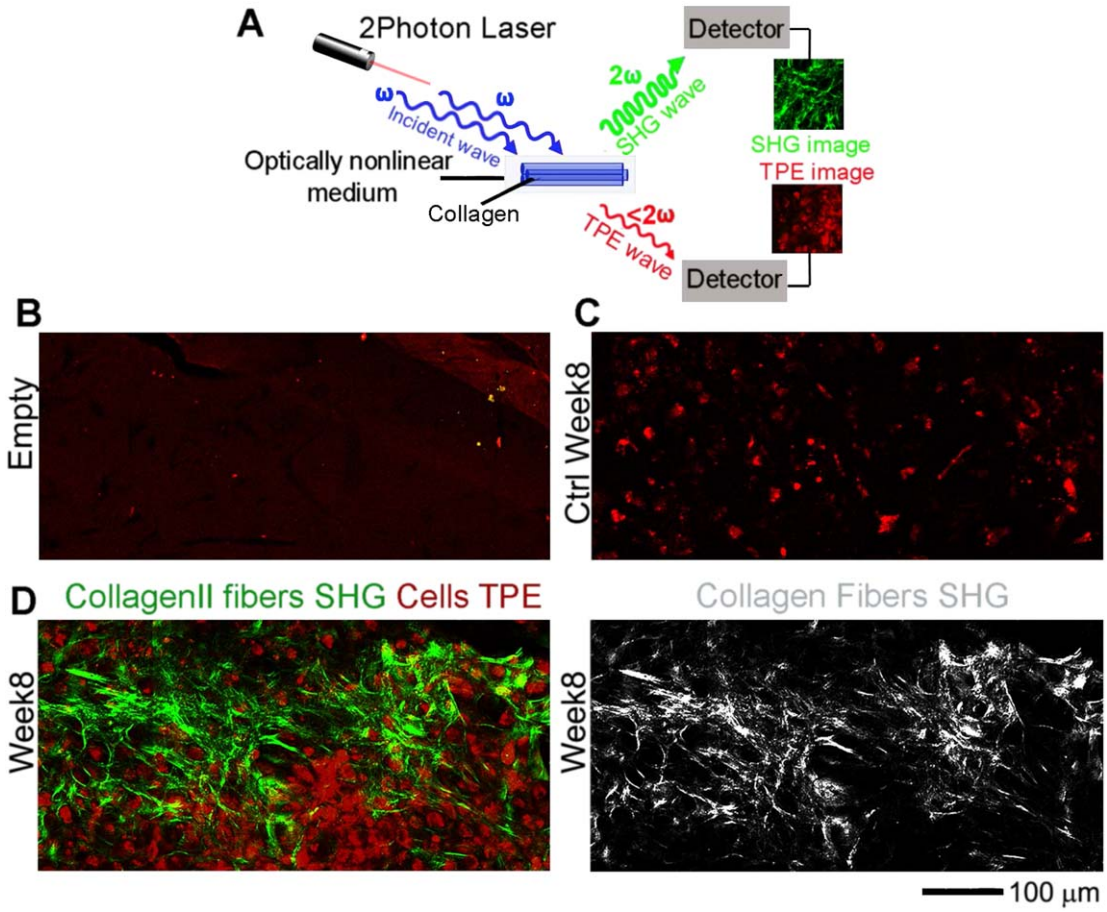

Figure 8. Neocartilage building and organization of collagen type II fibrils. (A) Schematic cartoon showing the nonlinear microscopy whereby dual-photon excitation gives rise to two-photon excitation (TPE) and second harmonic generation (SHG). Under dual-photon excitation conditions, non-centrosymmetric structures (such as collagen molecules) absorb and release energy in a different way to subcellular proteins. The light emitted from the excited non-centrosymmetric structures return at double energy, but half the wavelength of the original excitation photons generating images of the fibrillary structures of collagen proteins. (B) Representative image of the acellular control scaffold. (C) Representative images of hADCSs laden in GelMa/HAMa after 8 weeks in control media. (D) Representative images of hADCSs laden in GelMa/HAMa after 8 weeks of chondrogenic differentiation. Note: Samples have been fixed and cryosectioned and directly imaged for nonlinear microscopy (see Material and methods section for more detailed information).

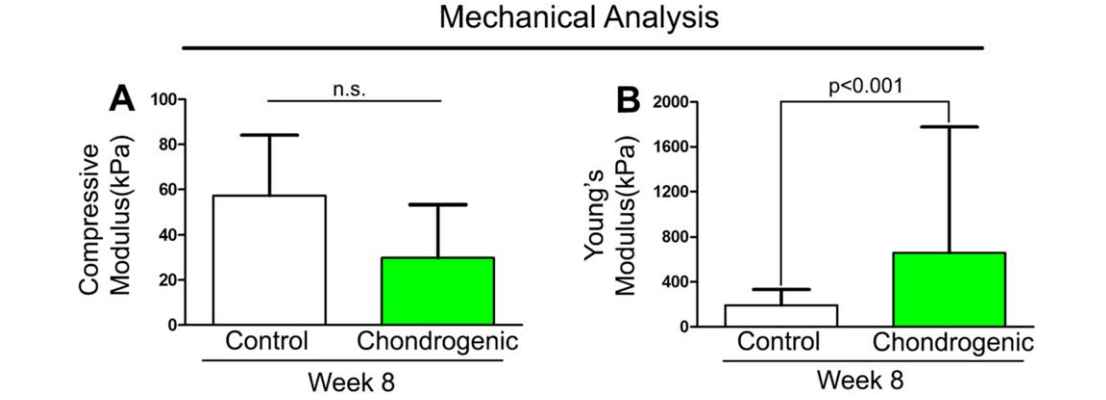

Figure 9. Mechanical properties evaluation. (A) The graph shows the unconfined compressive modulus of control and chondrogenic samples after 8 weeks. Error bars represents standard deviation between three biological replicates and significativity was calculated with unpaired t-test. (B) The graph indicates Young's modulus values obtained from analysing force curves using the Hertz indentation model of control and chondrogenic samples after 8 weeks. Error bars represents standard deviation between three biological replicates and significativity was calculated with unpaired t-test. These analyses have been performed on three hADSCs, undergoing chondrogenic differentiation, derived from three different patients.

patients affected by mild/severe OA, retain their chondrogenic potential, thus establishing the milestone for the treatment of cartilage injuries via using a personalized medicine approach using autologous stem cells [54]. Despite the heterogeneity of the clinical status of the patients, the data obtained showed consistent results among the different stem cells lines tested, defining our stem cells source, the human fat pad, as a good candidate for the clinical application.

In our previous study we have demonstrated that a core/shell distribution of our scaffold reliably protects the survival and proliferation capacity of hADSCs [31].

The co-axial extrusion approach have been proposed by other groups, they aimed to use a viscous sacrificial shell to allow the deposition of a liquid cellular compartment that cannot otherwise hold a predetermined shape, thus performing the hardening procedure before the removal of the sacrificial compartment [55–57].

The advantage of our technology relies instead on a different application of core/shell geometry. The segregation of the photocrosslinkable shell away from the cellular compartment, which is not photocrosslinked, is designed to protect the cells during the biofabrication process without compromising structural or cellular integrity. Our co-axial strategy geometrically compartmentalizes a solid phase that facilitates appropriate stiffness requirements, and a viscous liquid phase that preserves cell viability by separating cells from PIs and the cytotoxic chemical by-products coming from the crosslinking reaction going on within the solid phase. As shown in our previous study [31], the segregation of the core and shell compartments is well defined right after the biofabrication process.

Thus, we produced GelMa/HAMa bioscaffolds by means of Biopen mediated co-axial extrusion to assess whether the fabricated environment is permissive for neocartilage generation *in vitro*.

Expression of hyaline-like cartilage components was assessed first by RT-qPCR. SOX9, the master regulator of chondrogenesis, is expressed at transcriptional level but not at translational level before the chondrogenic induction, reflecting the chondrogenic potential of the stem cells source. However, SOX9 transcript accumulates over time under chondrogenic stimuli, reaching an expression plateau at week 4, with a consequent accumulation of the translated protein that continue to accumulate until week 8. This apparent discrepancy can be ascribed to the several post translational modification that regulates the stability of SOX9 in the cells. In fact, SOX9 is subjected to ubiquitin mediated proteasomal degradation effected by the E3 ubiquitin ligase FBW7 [58, 59] and by the E6 ubiquitin ligase UBE3A [60]. Moreover, the activation of TGFβ pathway leads to the stabilization of SOX9 by the phosphorylation of Serine 211 [61]. Thus, despite the transcriptional expression of SOX9 reaches a plateau, post translational modifications, triggered by chondrogenic stimuli, can positively affect the stability of the protein, leading to the activation of its transcriptional targets. In fact, COL2A1 and ACAN are not expressed at the start of the chondrogenesis, but are detectable at week 4 showing a 300 and 20 fold increase respectively at week 8. COL1A2, an accepted marker of fibrocartilage formation, is express in hADSCs populations and shows an increase of only 10 times over the entire length of chondrogenic stimulation. This is consistent with other studies that analysed the chondrogenic potential of 3D bioprinted hADSCs [42]. The production and accumulation of ECM containing Collagen type II, Proteoglycan and GAGs was demonstrated in a time-related manner both histologically and immunophenotypically. hADSCs secreted a significant amount of Collagen type II and Proteoglycan around the cell bodies and in the scaffold matrix. In contrast, no significant extracellular accumulation of Collagen type I was observed over time in the analysed bioscaffold. It has been shown that the ratio between Collagen type II and Collagen type I is the discriminant to define hyaline-like ECM [45]. After chondrogenic stimulation, the mentioned ratio is considerably higher in the GelMa/HAMa bioscaffolds both at transcriptional and translational level. Our settings are consistent with other studies showing Col II accumulation after 28 days of differentiation and performed using GelMa based bioinks and animal derived stem cells [62]. Moreover, the production of hyaline-like matrix we observed is highly efficient with respect to that generated from adult chondrocytes loaded in GelMa ink [63], underlining once again the superiority of hADSCs as a source of cells for the production of ECM in scaffold-based cartilage regeneration applications.

To further characterise our bioscaffolds, we have shown collagen fibrils formation and distribution using nonlinear two photon microscopy and SHG [64, 65]. This technique can detect only mature fibrillary collagen. Our results showed that Collagen type I and X are expressed at the intracellular level. In contrast, Collagen II are secreted and accumulated in an organized ECM after 8 weeks of chondrogenesis. Thus, is very likely that mature Collagen II is the major contributor of the SHG signal.

The pattern of matrix deposition in bioscaffolds resembles the early stages formation of the growth plate with an accumulation of collagen type II in the surface of the developing tissue. It is in fact well established that cartilage formation begins with mesenchymal condensation leading to chondrogenic differentiation of mesenchymal cells. Then, a dense matrix is produced, serving as the cartilage anlage, a template for the subsequent generation of both the articular cartilage and the subchondral bone [48, 49]. The formation of physiologic tissue by progenitor cells ultimately required lessons taken from native tissue morphogenesis. Self-assembly has been proposed as an *in vitro* method for recapitulating mesenchymal

condensation that precedes chondrogenesis [66]. However current tissue-engineered scaffolds for chondrogenesis pay little attention to this phenomenon or focused more on the modification of the bioink by adding growth factors or decellularized ECM components to help the cellular condensation [67], while others use cells pre-clustered into pellets prior to 3D manufacturing to mimic the mesenchymal condensation [68]. With our setting instead, we demonstrated that hADSCs are able to condense under *in vitro* chondrogenic stimulation and successfully produce hyaline-like bioscaffolds. Moreover, the peripheral distribution of matrix formation is promising in the view of the entire osteochondral tissue regeneration. In the future, the possibility to deliver a gradient of osteogenic and chondrogenic growth factors within the hydrogel could promote the selective tissue differentiation allowing the formation of bone and cartilage simulating the entire osteochondral unit [69]. Importantly, our culture technique was performed in a static fashion, therefore not stimulating the orientation of the collagen fibres in a way to recapitulate hyaline-like cartilage structures. To better simulate the physiological environment within the joint, the use of a dynamic culture systems will be necessary to improve the orientation of the collagen fibres, as shown in previous studies [70]. Mechanical resistance to stress is undoubtedly a key element in cartilage tissue engineering: just like native articular cartilage, the regenerated tissue needs to be able to sustain the loads applied on the joint and distribute them evenly in the underlying subchondral bone. There is currently no consensus on the expected results from mechanical testing following cartilage regeneration in hydrogels. While several studies have shown that after 4 or 8 weeks in chondrogenic culture media, 3D printed samples show increase in the compression modulus [71], other studies show decrease or stagnation of mechanical properties with time in compression [72], and in tension [73]. In our study, by unconfined compression tests, we found no statistically significant difference of the bulk mechanical properties between chondrogenic bioscaffolds and their control counterparts. Importantly, several studies aiming at cartilage matrix growth in hydrogels demonstrated a compressive modulus after 8 weeks reaching about 50 kPa [71, 72, 74], which is the constant modulus of our hydrogel. While this compressive modulus is achieved during the chondrogenic process *in vitro*, with our approach it is possible to obtain a comparable stiffness right after the biofabrication process. The mechanical behaviour of the bioscaffolds is determined by the interplay between intrinsic degradation of the biomaterial components, cell mediated degradation and ECM deposition [75]. However, by performing atomic force microscopy indentation, we have demonstrated that in correspondence of accumulated ECM there is a marked increase in Young's modulus at 8 weeks of chondrogenesis, compared to undifferentiated samples. This analysis highlights the importance of considering spatial variations in constructs. These results reflect the fact that ECM accumulation lead to a gain in mechanical resistance in localized regions that correspond to the area of where cell condensation happens. In our next studies, the phenotype and migration of the cells, matrix deposition, proteolytic activity and construct degradation rate will be evaluated and correlated with de novo cartilage formation to better understand the interaction between hADSCs and crosslinked GelMa/HAMa hydrogel [76].

5. Conclusion

The clinical application of hydrogel based bioscaffolds has the potential to effect the regeneration of articular cartilage. In this study, we have demonstrated that human IPFP adipose-derived stem cells can produce hyaline-like cartilage in GelMa/HAMa bioscaffolds. The *in vitro* biofabrication of human neocartilage via a handheld extrusion device is a key step in the path towards the development of tissue regeneration strategies in the clinical practice.

Acknowledgments

This work was supported by (1) Arthritis Australia—Zimmer Australia Grant, (2) Victorian Orthopaedic Research Trust, (3) The John Loewenthal Foundation for Surgery (Royal Australasian College of Surgeons), (4) The Australian Research Council Centre of Excellence Scheme (Project Number CE 140100012), and (5) St Vincent's Hospital (Melbourne).

Research Endowment Found. Equipment Grant form MTPConnect is gratefully acknowledged. Access to atomic force microscope facilities was provided through the Materials Characterisation and Fabrication Platform at the University of Melbourne.

The authors would like to thank the Australian National Nanofabrication Facility—Materials node for equipment use; Dr Andre Tan for technical assistance in performing SHG microscopy. Confocal Microscopy and IMARIS software usage were performed at the Biological Optical Microscopy Platform, The University of Melbourne

(www.microscopy.unimelb.edu.au).

Author contributions statement

CO, SD designed and performed the experiments, executed the data analyses, wrote the manuscript and prepared the figures.

CO'C design the analyses, performed the AFM tests, gave intellectual input throughout the project, and reviewed the manuscript draft.

RB performed and analysed the compression testing analysis as well as gave intellectual input throughout the project, and reviewing of the manuscript draft.

AJO provided intellectual input and edited the manuscript.

MS performed the image acquisition with light sheet microscope.

GGW and PFMC conceived the idea of the surgical handheld device, have been involved in development of concept, edited and approved manuscript.

CDB designed the overall project, supervised the experiments, analysed and interpreted the data, wrote the manuscript and approved the final version.

All authors approved the final manuscript.

Author disclosure statement

We declare that this manuscript is original, has not been published before and is not currently being considered for publication elsewhere. We wish to confirm that there are no conflicts of interest associated with this publication and there have been no competing financial interests for this work that could have influenced its outcome.

We confirm that the manuscript has been read and approved by all named authors and that there are no other persons who satisfied the criteria for authorship but are not listed. We further confirm that all of us have approved the order of authors listed in the manuscript.

We confirm that we have given due consideration to the protection of intellectual property associated with this work and that are no impediments to publication, including the timing of publication, with respect to intellectual property. In so doing we confirm that we have followed the regulations of our institutions concerning intellectual property.

Ethical statement

St. Vincent Hospital Ethics Committee [HREC/16/SVHM/186] approved use of all human samples and procedures (isolation of hADSCs from human infrapatellar fat pad) in this study and all the experiments were performed in accordance with relevant guidelines and regulations.

ORCID iDs

Carmine Onofrillo https://orcid.org/0000-0003-2537-6672

References

[1] Hollander A P, Dickinson S C and Kafienah W 2010 Stem cells and cartilage development: complexities of a simple tissue *Stem Cells* **28** 1992–6

[2] Muiznieks L D and Keeley F W 2013 Molecular assembly and mechanical properties of the extracellular matrix: a fibrous protein perspective *Biochim. Biophys. Acta—Mol. Basis Dis.* **1832** 866–75

[3] Mansour J M 2009 Biomechanics of cartilage *Kinesiology: The Mechanics and Pathomechanics of Human Movement* ed C A Oatis 2nd edn (Philadelphia, PA: Wolters Kluwer Health) pp 66–79

[4] Kon E, Filardo G, Di Martino A and Marcacci M 2012 ACI and MACI *J. Knee Surg.* **25** 017–22

[5] Makris E A, Gomoll A H, Malizos K N, Hu J C and Athanasiou K A 2016 Repair and tissue engineering techniques for articular cartilage *Nat. Rev. Rheumatol.* **11** 21–34

[6] Wood J J, Malek M A, Frassica F J, Polder J A, Mohan A K, Bloom E D A T, Braun M M and Coté T R 2006 Autologous cultured chondrocytes: adverse events reported to the united states food and drug administration *J. Bone Joint Surg. Am.* **88** 503-7

[7] Lin Z, Fitzgerald J B, Xu J, Willers C, Wood D, Grodzinsky A J and Zheng M H 2008 Gene expression profiles of human chondrocytes during passaged monolayer cultivation *J. Orthop. Res.* **26** 1230–7

[8] Dewan A K, Gibson M A, Elisseeff J H and Trice M E 2014 Evolution of autologous chondrocyte repair and comparison to other cartilage repair techniques *Biomed Res. Int.* **2014** 272481

[9] Deng Z, Jin J, Zhao J and Xu H 2016 Cartilage defect treatments: with or without cells? Mesenchymal stem cells or chondrocytes? Traditional or matrix-assisted? A systematic review and meta-analyses *Stem Cells Int.* **2016** 9201492

[10] Goldring M B and Goldring S R 2010 Articular cartilage and subchondral bone in the pathogenesis of osteoarthritis *Ann. NY Acad. Sci.* **1192** 230–7

[11] Omori G 2005 Epidemiology of knee osteoarthritis *Acta Med. Biol.* **53** 1–11

[12] Vos T *et al* 2012 Years lived with disability (YLDs) for 1160 sequelae of 289 diseases and injuries 1990–2010: a systematic analysis for the Global Burden of Disease Study 2010 *Lancet* **380** 2163–96

[13] Ondrésik M *et al* 2017 Management of knee osteoarthritis. Current status and future trends *Biotechnol. Bioeng.* **114** 717–39

[14] Baugé C and Boumédiene K 2015 Use of adult stem cells for cartilage tissue engineering: current status and future developments *Stem Cells Int.* **2015** 438026

[15] Martin I, Ireland H, Baldomero H and Passweg J 2015 The survey on cellular and engineered tissue therapies in Europe in 2012 *Tissue Eng.* A **21** 1–13

[16] Cornelissen D-J, Faulkner-Jones A and Shu W 2017 Current developments in 3D bioprinting for tissue engineering *Curr. Opin. Biomed. Eng.* **2** 76–82

[17] Liu Y, Zhou G and Cao Y 2017 Recent progress in cartilage tissue engineering—our experience and future directions *Engineering* **3** 28–35

[18] Daly A C, Freeman F E, Gonzalez-Fernandez T, Critchley S E, Nulty J and Kelly D J 2017 3D bioprinting for cartilage and osteochondral tissue engineering *Adv. Healthc. Mater.* **6** 1–20

[19] Di Bella C, Fosang A, Donati D M, Wallace G G and Choong P F M 2015 3D bioprinting of cartilage for orthopedic surgeons: reading between the lines *Front. Surg.* **2** 1–7

[20] Iwasa J, Engebretsen L, Shima Y and Ochi M 2009 Clinical application of scaffolds for cartilage tissue engineering *Knee Surg., Sports Traumatol. Arthrosc.* **17** 561–77

[21] Kang H-W, Yoo J J and Atala A 2015 *Bioprinted Scaffolds for Cartilage Tissue Engineering BT—Cartilage Tissue Engineering: Methods and Protocols* ed P M Doran (New York: Springer) pp 161–9

[22] Rai V, Dilisio M F, Dietz N E and Agrawal D K 2017 Recent strategies in cartilage repair: a systemic review of the scaffold development and tissue engineering *J. Biomed. Mater. Res.* A **105** 2343–54

[23] Koh J L, Wirsing K, Lautenschlager E and Zhang L-O 2004 The effect of graft height mismatch on contact pressure following

osteochondral grafting: a biomechanical study *Am. J. Sports Med.* **32** 317–20
[24] Mollon B, Kandel R, Chahal J and Theodoropoulos J 2013 The clinical status of cartilage tissue regeneration in humans *Osteoarthr. Cartil.* **21** 1824–33
[25] Keriquel V, Guillemot F, Arnault I, Guillotin B, Miraux S, Amédée J, Fricain J-C and Catros S 2010 *In vivo* bioprinting for computer-and robotic-assisted medical intervention: preliminary study in mice *Biofabrication* **2** 014101
[26] Ozbolat I T 2018 Bioprinting scale-up tissue and organ constructs for transplantation *Trends Biotechnol.* **33** 395–400
[27] Schmutzer M and Aszodi A 2017 Cell compaction influences the regenerative potential of passaged bovine articular chondrocytes in an *ex vivo* cartilage defect model *J. Biosci. Bioeng.* **123** 512–22
[28] Bartz C, Meixner M, Giesemann P, Roël G, Bulwin G-C and Smink J J 2016 An *ex vivo* human cartilage repair model to evaluate the potency of a cartilage cell transplant *J. Transl. Med.* **14** 317
[29] O'Connell C D *et al* 2016 Development of the Biopen: a handheld device for surgical printing of adipose stem cells at a chondral wound site *Biofabrication* **8** 015019
[30] Di Bella C *et al In situ* handheld three-dimensional bioprinting for cartilage regeneration *J. Tissue Eng. Regen. Med.* **12** 611–21
[31] Duchi S *et al* 2017 Handheld co-axial bioprinting: application to *in situ* surgical cartilage repair *Sci. Rep.* **7** 1–12
[32] Moyad T F 2011 Cartilage injuries in the adult knee: evaluation and management *Cartilage* **2** 226–36
[33] Ye K, Felimban R, Traianedes K, Moulton S E, Wallace G G, Chung J, Quigley A, Choong P F M and Myers D E 2014 Chondrogenesis of infrapatellar fat pad derived adipose stem cells in 3D printed chitosan scaffold *PLoS One* **9** e102638
[34] Estes B T, Diekman B O, Gimble J M and Guilak F 2010 Isolation of adipose-derived stem cells and their induction to a chondrogenic phenotype *Nat. Protocols* **5** 1294–311
[35] Felimban R, Ye K, Traianedes K, Di Bella C, Crook J, Wallace G G, Quigley A, Choong P F M and Myers D E 2014 Differentiation of stem cells from human infrapatellar fat pad: characterization of cells undergoing chondrogenesis *Tissue Eng.* A **20** 1–11
[36] Lucarelli E *et al* 2014 *In vitro* biosafety profile evaluation of multipotent mesenchymal stem cells derived from the bone marrow of sarcoma patients *J. Transl. Med.* **12** 95
[37] Loessner D, Meinert C, Kaemmerer E, Martine L C, Yue K, Levett P A, Klein T J, Melchels F P W, Khademhosseini A and Hutmacher D W 2016 Functionalization, preparation and use of cell–laden gelatin methacryloyl-based hydrogels as modular tissue culture platforms *Nat. Protocols* **11** 727–46
[38] Knudson C B 2003 Hyaluronan and CD44: strategic players for cell–matrix interactions during chondrogenesis and matrix assembly *Birth Defects Res.* C **69** 174–96
[39] Barry F and Murphy M 2013 Mesenchymal stem cells in joint disease and repair *Nat. Rev. Rheumatol.* **9** 584–94
[40] Du D, Sugita N, Liu Z, Moriguchi Y, Nakata K, Myoui A and Yoshikawa H 2015 Repairing osteochondral defects of critical size using multiple costal grafts: an experimental study *Cartilage* **6** 241–51
[41] Katagiri H, Mendes L F and Luyten F P 2017 Definition of a critical size osteochondral knee defect and its negative effect on the surrounding articular cartilage in the rat *Osteoarthr. Cartil.* **25** 1531–40
[42] Squitieri L 2005 *Method for quantitative analysis of glycosaminoglycans and type II collagen in chondrocyte-seeded articular cartilage scaffolds with varied cross-linking density* Undergraduate ThesisMassachusetts Institute of Technology http://hdl.handle.net/1721.1/32924
[43] Bi W, Deng J M, Zhang Z, Behringer R R and de Crombrugghe B 1999 SOX9 is required for cartilage formation *Nat. Genet.* **22** 85
[44] Bi W, Huang W, Whitworth D J, Deng J M, Zhang Z, Behringer R R and de Crombrugghe B 2001 Haploinsufficiency of SOX9 results in defective cartilage primordia and premature skeletal mineralization *Proc. Natl Acad. Sci. USA* **98** 6698–703
[45] Marlovits S, Hombauer M, Truppe M, Vècsei V and Schlegel W 2004 Changes in the ratio of type-I and type-II collagen expression during monolayer culture of human chondrocytes *Bone Joint J.* **86-B** 286–95
[46] Daly A C , Chritcley S E, Rencsok E M and Kelly D J 2016 A comparison of different bioinks for 3D bioprinting of fibrocartilage and hyaline cartilage *Biofabrication* **8** 045002
[47] Yourek G, Hussai M A and Mao J J 2014 Cytoskeletal changes of mesenchymal stem cells during differentiation *ASAIO J.* **53** 219–28
[48] Shimizu H, Yokoyama S and Asahara H 2007 Growth and differentiation of the developing limb bud from the perspective of chondrogenesis *Dev. Growth Differ.* **49** 449–54
[49] Olsen B R, Reginato A M and Wang W 2000 Bone development *Annu. Rev. Cell Dev. Biol.* **16** 191–220
[50] Wang M *et al* 2017 Advances and prospects in stem cells for cartilage regeneration *Stem Cells Int.* **2017** 4130607
[51] Savkovic V, Li H, Seon J K, Hacker M, Franz S and Simon J C 2014 Mesenchymal stem cells in cartilage regeneration *Curr. Stem Cell Res. Ther.* **9** 469–88
[52] Lee W Y and Wang B 2017 Cartilage repair by mesenchymal stem cells: clinical trial update and perspectives *J. Orthop. Transl.* **9** 76–88
[53] do Amaral R J F C, Almeida H V, Kelly D J, O'Brien F J and Kearney C J 2017 Infrapatellar fat pad stem cells: from developmental biology to cell therapy *Stem Cells Int.* **2017** 6843727
[54] Sawitzke A D 2013 Personalized medicine for osteoarthritis: where are we now? *Ther. Adv. Musculoskelet. Dis.* **5** 67–75
[55] Gao Q, He Y, Fu J, Liu A and Ma L 2015 Coaxial nozzle-assisted 3D bioprinting with built-in microchannels for nutrients delivery *Biomaterials* **61** 203–15
[56] Colosi C, Shin S R, Manoharan V, Massa S, Costantini M, Barbetta A, Dokmeci M R, Dentini M and Khademhosseini A 2016 Microfluidic bioprinting of heterogeneous 3D tissue constructs using low-viscosity bioink *Adv. Mater.* **28** 677–84
[57] Costantini M, Idaszek J, Szöke K, Jaroszewicz J, Dentini M, Barbetta A, Brinchmann J E and Święszkowski W 2016 3D bioprinting of BM-MSCs-loaded ECM biomimetic hydrogels for *in vitro* neocartilage formation *Biofabrication* **8** 035002
[58] Suryo Rahmanto A *et al* 2016 FBW7 suppression leads to SOX9 stabilization and increased malignancy in medulloblastoma *EMBO J.* **35** 2192–212
[59] Hong X *et al* 2016 SOX9 is targeted for proteasomal degradation by the E3 ligase FBW7 in response to DNA damage *Nucleic Acids Res.* **44** 8855–69
[60] Hattori T, Kishino T, Stephen S, Eberspaecher H, Maki S, Takigawa M, de Crombrugghe B and Yasuda H 2013 E6-AP/UBE3A protein acts as a ubiquitin ligase toward SOX9 protein *J. Biol. Chem.* **288** 35138–48
[61] Coricor G and Serra R 2016 TGF-β regulates phosphorylation and stabilization of SOX9 protein in chondrocytes through p38 and Smad dependent mechanisms *Sci. Rep.* **6** 38616
[62] Levato R, Webb W R, Otto I A, Mensinga A, Zhang Y, van Rijen M, van Weeren R, Khan I M and Malda J 2017 The bio in the ink: cartilage regeneration with bioprintable hydrogels and articular cartilage-derived progenitor cells *Acta Biomater.* **61** 41–53
[63] Schuurman W, Levett P A, Pot M W, van Weeren P R, Dhert W J A, Hutmacher D W, Melchels F P W, Klein T J and Malda J 2013 Gelatin-methacrylamide hydrogels as potential biomaterials for fabrication of tissue-engineered cartilage constructs *Macromol. Biosci.* **13** 551–61
[64] Zipfel W R, Williams R M and Webb W W 2003 Nonlinear magic: multiphoton microscopy in the biosciences *Nat. Biotechnol.* **21** 1369
[65] Zoumi A, Lu X, Kassab G S and Tromberg B J 2004 Imaging coronary artery microstructure using second-harmonic and two-photon fluorescence microscopy *Biophys. J.* **87** 2778–86
[66] Pacifici M, Koyama E, Shibukawa Y, Wu C, Tamamura Y, Enomoto-Iwamoto M and Iwamoto M 2006 Cellular and molecular mechanisms of synovial joint and articular cartilage formation *Ann. NY Acad. Sci.* **1068** 74–86

[67] Kim I G, Ko J, Lee H R, Do S H and Park K 2016 Mesenchymal cells condensation-inducible mesh scaffolds for cartilage tissue engineering *Biomaterials* **85** 18–29
[68] Suzuki S, Muneta T, Tsuji K, Ichinose S, Makino H, Umezawa A and Sekiya I 2012 Properties and usefulness of aggregates of synovial mesenchymal stem cells as a source for cartilage regeneration *Arthritis Res. Ther.* **14** R136
[69] Censi R, Matricardi A D and Pietro 2015 Bioactive hydrogel scaffolds—advances in cartilage regeneration through controlled drug delivery *Curr. Pharm. Des.* **21** 1545–55
[70] El-Ayoubi R, DeGrandpré C, DiRaddo R, Yousefi A-M and Lavigne P 2009 Design and dynamic culture of 3D-scaffolds for cartilage tissue engineering *J. Biomater. Appl.* **25** 429–44
[71] Chung C, Beecham M, Mauck R L and Burdick J A 2009 The influence of degradation characteristics of hyaluronic acid hydrogels on *in vitro* neocartilage formation by mesenchymal stem cells *Biomaterials* **30** 4287–96
[72] Roberts J J, Nicodemus G D, Greenwald E C and Bryant S J 2011 Degradation improves tissue formation in (un)loaded chondrocyte-laden hydrogels *Clin. Orthop. Relat. Res.* **469** 2725–34
[73] Duan B, Hockaday L A, Kang K H and Butcher J T 2013 3D Bioprinting of heterogeneous aortic valve conduits with alginate/gelatin hydrogels *J. Biomed. Mater. Res.* A **101A** 1255–64
[74] Marrella A, Lagazzo A, Barberis F, Catelani T, Quarto R and Scaglione S 2017 Enhanced mechanical performances and bioactivity of cell laden-graphene oxide/alginate hydrogels open new scenario for articular tissue engineering applications *Carbon* **115** 608–16
[75] Kim K, Yoon D M, Mikos A G and Kasper F K 2012 Harnessing cell–biomaterial interactions for osteochondral tissue regeneration BT *Tissue Engineering III: Cell–Surface Interactions for Tissue Culture* ed C Kasper *et al* (Berlin: Springer) pp 67–104
[76] Sarem M, Arya N, Heizmann M, Neffe A T, Barbero A, Gebauer T P, Martin I, Lendlein A and Shastri V P 2018 Interplay between stiffness and degradation of architectured gelatin hydrogels leads to differential modulation of chondrogenesis *in vitro* and *in vivo Acta Biomater.* **69** 83–94